THERMIONIC REFRIGERATION WITH PLANAR AND NONPLANAR ELECTRODES - CHANCES AND LIMITS -

Y.-C. Gerstenmaier, G. Wachutka

Belgirate, Italy, 28-30 September 2005

THERMIONIC REFRIGERATION WITH PLANAR AND NONPLANAR ELECTRODES - CHANCES AND LIMITS -

Y.C. Gerstenmaier and G. Wachutka***

*Siemens AG, Corporate Technology, D-81730 Muenchen, Germany, e-mail: yge@tep.ei.tum.de
**Institute for Physics of Electrotechnology, Munich University of Technology

ABSTRACT

In this paper for the first time a precise theoretical analysis of efficiencies and power densities for nano-scaled thermionic vacuum gap devices is presented. Plane electrodes with nano-gaps will be treated first. With nonplanar electrodes (nanotips) enhanced electron field emission occurs, giving rise to new design options. The theories of field and thermionic emission are combined by calculating the transmission coefficient for the surface potential barrier exactly numerically for thermionic and tunnelling energies. This then is used for current and energy transport determination and derivation of cooling and generator efficiencies. Because of the high work function of metals, efficient thermionic electron emission takes place only at high temperatures. At low temperatures also efficiencies near Carnot are possible but with very low power densities. The energy exchange processes in the cathode during emission are reviewed and an improved model is presented.

1. INTRODUCTION

With increasing power densities in micro- and power-electronic components thermoelectric cooling becomes more and more interesting [1], [2]. Contrary to the traditional cooling of PCBs and modules by fans or radiators, thermoelectric devices can cool in a controlled way in the immediate neighbourhood of the hot spots of the power dissipating devices. Especially in opto-electronic devices very high power densities occur over a small region. However, the efficiency (coefficient of performance = CoP) of coolers with bulk thermoelectric materials is still low. The figure of merit for these materials $Z\,T = S^2\,\sigma\,T\,/\lambda$ with S the thermo-power (Seebeck coefficient), σ the electrical conductivity, λ the thermal conductivity and T the average temperature between the high temperature side T_H and cold temperature side T_C of the device does not exceed 1 very much [3], [4]. In an inverse mode of operation thermoelectric and thermionic devices can also be used as generators. A large demand of micro-structured generators [5] and coolers is expected in the telecommunication sector.

In recent years considerable progress has been made in the development of thermoelectric nano-structured superlattices [1, 6, 7, 8]. *ZT* values of 2.4 have been achieved for phonon blocking lattices [7] (low thermal conductivity) with temperature gradient and current flow perpendicular to the planes of the multilayer structure. Even higher *ZT* values of 3.8 were obtained for quantum well confinement multilayer structures with temperature gradient and current transport parallel to the planes [8] (low dimensional or 2D system).

The purpose of this work is to investigate theoretically the potential of thermionic vacuum devices with additional electron field emission due to non planar electrodes for cooling applications. Because of the high work function of metals, thermionic electron emission (i.e. by thermal excitation of electrons) takes place only at very high temperatures over 1500 K. Thermionic generators, e.g. for space missions, are known for long [9]. In [10, 11] thermionic devices with plane electrodes were also proposed and calculated for cooling. Figure 1 shows the band structure over a vacuum barrier with applied voltage V between cathode and anode and work function *W*. The electron to be emitted must have an energy higher than the electrochemical potential μ (equal to the Fermi energy E_F at T = 0°K) plus *W*. The line in the vacuum gap indicates the lowest possible energy level for the electron there and gives the electric field by its gradient. Electrons with high energy, evaporating from the cathode, reduce the average electron energy and cool the cathode. For operation at room temperatures work functions as low as 0.3eV are needed, which cannot be achieved at present. For operation at 500K 0.7eV would be sufficient. The potential barrier *W* is considerably lower in solid state hetero-junctions or for barriers caused by pn-doping [12, 13, 6]. In case of sufficiently thin barriers ballistic electron transport (i.e. without scattering) occurs between cathode and anode which has been analysed in [14] by Monte Carlo simulation. For broader solid state barriers there is no clear-cut dividing line between thermionic cooling and thermoelectric Peltier cooling. On the other hand, the efficiency of solid state devices is reduced compared to vacuum gap devices due to the heat Fourier current over the barrier. In [15] it has been pointed out, that it may be important to consider the Joule losses in the cathode and its contact resistance for an overall efficiency calculation.

When using a vacuum gap, operation at room temperature

ISBN 2-916187-01-4

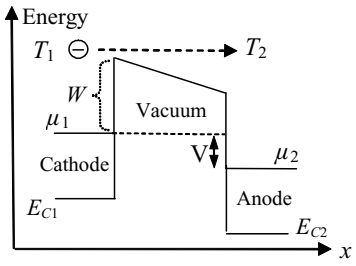

Figure 1: Thermionic emission over vacuum potential barrier with applied voltage V. E_C is the bottom of the conduction band, μ the Fermi-level, W workfunction.

and below is conceivable by reducing the electrodes spacing to a few nm so that quantum mechanical tunnelling becomes possible also for lower cathode temperature. A theoretical analysis was presented in [16]. As a result it turned out that the electrodes spacing has to be larger than 4nm. Otherwise excessive tunnelling of electrons from below the Fermi level would occur, which leads to heating of the cathode instead of cooling, because then the average electron energy increases. The CoP of such devices could be high and their realisation is pursued since several years [17, 18]. However, the feasibility of the nano-gap concept with planar electrodes is not proved and doubts concerning their realisation are not cleared up.

We shall analyse vacuum nano-gap devices with plane electrodes more precisely in section 5, both, for refrigeration and current generation, following the theory developed in section 2 and 3. In section 6 the performance of enhanced field emission devices with arrays of nanotips at the emitting electrode will be investigated and compared.

2. THEORY OF ELECTRON EMISSION

In the usual theory of electron field emission [27, 28, 29] the Sommerfeld free electron model is used, which is a good approximation for metals. To treat semiconductors this formalism should be extended to electrons in a periodic effective crystal potential using Bloch wave functions. The energy bands $\mathcal{E}_n(\mathbf{k})$ can in principle be obtained by bandstructure calculations. Here n denotes the band index and $\hbar\mathbf{k}$ the crystal momentum of the single electron, not to be confused with its real momentum. In the interior of the material at thermal equilibrium the number of electrons per unit volume in states around $\mathbf{k}$ in a volume element d^3k is according to Fermi-Dirac statistics:

$$f(\mathcal{E}_n(\mathbf{k}))\ d^3k/4\pi^3 = \left(\exp(\mathcal{E}_n(\mathbf{k})-\mu)/k_BT)+1\right)^{-1}\ d^3k/4\pi^3 \quad (1)$$

where $1/\ 8\pi^3$ is the density of levels for the unit $\mathbf{k}$-volume. (Each level can be occupied by two electrons.) For current transport in the presence of electric fields and temperature gradients the Fermi distribution would have to be replaced by a non-equilibrium distribution function $g(\mathbf{r}, \mathbf{k})$ depending generally also on position $\mathbf{r}$. Often the relaxation time approximation with a semiclassical model of electron dynamics is used in calculating g [30, p. 244]:

$$g(\mathbf{r},\mathbf{k}) = f(\mathcal{E}(\mathbf{k})) - e\mathbf{F}(\mathbf{r})\cdot\mathbf{v}(\mathbf{k})\ \tau(\mathcal{E}(\mathbf{k}))\frac{\partial f(\mathcal{E}(\mathbf{k}))}{\partial\mathcal{E}} - \mathbf{v}(\mathbf{k})\cdot\nabla T(\mathbf{r})\ \tau(\mathcal{E}(\mathbf{k}))\frac{\partial f(\mathcal{E}(\mathbf{k}))}{\partial T} \quad (2)$$

where $\mathbf{F}$ is the applied external electric field, $\mathbf{v}$ is the expectation value of the electron's velocity, $\tau(\mathcal{E})$ is the relaxation time and ∇T is the temperature gradient. e denotes the magnitude of the electron charge. Expression (2) can be justified, when the single electron is described by a wave packet of Bloch wave functions extending over many crystal grid cells. On the other hand the extension of the wave packet has to be smaller than the length over which the external electric field varies appreciably. These conditions are no longer satisfied at the surface, where strong potential variations according to fig.1 occur on a scale of the lattice constant.

The concept of effective electron mass and crystal momentum are attributes of a quasi-particle not subject to the crystal potential - which has been accounted for by use of the Bloch waves - but only to a slowly varying external potential. The potential step W at the surface is caused by a dipole layer of width not more than a lattice constant. In calculating the transmission of the electrons through this barrier the original crystal potential is essential and the effective mass concept cannot be used any longer. For the electrons impinging on the surface barrier from inside the metal therefore the real electron mass has to be used. In [31] it is argued, that in the transmission of heterojunction potential barriers the smaller effective mass of the two materials has to be used.

Since there is no consistent theory for current and energy transport over the surface barrier, several heuristic approaches are used in the literature. We start on a more general basis by considering an electron current impinging on a surface element dS from inside the material. The normal direction perpendicular to dS will be denoted in local coordinates as x-direction. The probability for an electron impinging with velocity component $v_x > 0$ to tunnel through the surface potential barrier $V(\mathbf{r})$ will be denoted by $D(v_x)$, where v_x is the x-component of the expectation value of the velocity. According to Bloch's theory: $\boldsymbol{v}(\mathbf{k}) = \nabla_{\mathbf{k}}\,\mathcal{E}_n(\mathbf{k})\ /\hbar$. Since electron density times v_x gives the current density normal to the surface, the total emission current density can be written with the help of (1) by integration over all electron states in k-space with $v_x(\mathbf{k}) > 0$:

$$J_e = e\int_{\mathbf{k},\,v_x(\mathbf{k})>0} D(v_x(\mathbf{k}))\frac{\partial\mathcal{E}_n(\mathbf{k})/\partial\mathbf{k}_x}{\hbar}f(\mathcal{E}_n(\mathbf{k}))\frac{d^3k}{4\pi^3}\cdot \quad (3)$$

In this work electron current will be defined to be in the direction of the particle flow, opposite to the technical direction of electrical current. In (3) the non-equilibrium distribution g can be approximated by the equilibrium f near the surface, which is a good approximation.

Restricting for the time being to the free electron model with real electron mass m and real momentum $\hbar\mathbf{k}$, because of lack of bandstructure data, $\mathcal{E}_n(\mathbf{k})$ reduces to

$$\mathcal{E}_n(\mathbf{k}) = E_C + (\hbar\mathbf{k})^2/2m\ , \quad (4)$$

 ISBN 2-916187-01-4

where E_C is the energy of the bottom of the conduction band which can be chosen to be zero.

By use of the expression (4) in (3) the electron's velocity in x-direction becomes: $v_x = \hbar\, k_x / m$. E_x will denote the x-component $m\, v_x^2 /2 = (\hbar k_x)^2/2m$ of the total kinetic energy $E(k) = mv^2/\,2 = (\hbar k)^2/2m$. The integration in (3) is thus reduced to **k**-values with $k_x > 0$. With $k^2 = k_x^2 + k_y^2 + k_z^2$:

$$J_e = e\int_{k_x>0}\int_{k_y}\int_{k_z} D(E_x(k_x))\,\frac{\hbar k_x}{m}\, f(E_C + E(k))\,\frac{d^3k}{4\pi^3}\,. \quad (5)$$

The 3D integral in (5) can be simplified by a suitable parameter transformation using kinetic energy E and its x-component E_x as independent variables. Eq. (5) then reads:

$$J_e = \frac{4\pi\, me}{h^3}\int_0^\infty f(E_C + E)\left(\int_0^E D(E_x)dE_x\right)dE \quad (6)$$

This result was also obtained in other context in [28] and is used in [32]. It can be proved in a more compact way by rewriting d^3k in polar coordinates and using the definitions of $E(k)$ and E_x . The integrand of (6) is the differential emission current density

$$j(E) = \frac{4\pi\, me}{h^3}\, f(E_C + E)\int_0^E D(E_x)\, dE_x$$

and can be interpreted as the current density $j(E)\,\mathrm{d}E$ in the energy range between E and $E+\mathrm{d}E$ originating from all electron directions inside the material. The corresponding particle flux is obtained by division by e .

In order to obtain the emitted energy current density, the particle flux is weighted with the total energy $E + E_C$:

$$J_E = \frac{4\pi\, m}{h^3}\int_0^\infty f(E_C + E)(E_C + E)\left(\int_0^E D(E_x)\, dE_x\right)dE \quad (7)$$

The classical work of [29] considered one dimensional electron emission in the free electron model from a plane surface with constant external electric field F thus resulting in a triangular shaped potential vacuum barrier: $V(x) = (W + \mu) - e\,F\,x$, where x is the distance from the surface. Nowadays the term Fowler-Nordheim tunnelling is often used generally for tunnelling across triangular shaped barriers. It is essential to include in $V(x)$ also the Schottky image potential $-e^2/\,4x$ caused by the redistribution of charges on the metal surface induced by a single electron in the vacuum, which lowers the maximum $W + \mu$ of V to a certain degree.

Both, for tunnelling and pure thermionic emission at high energies (temperatures), the transmission coefficient $D(E_x)$ for a potential barrier $V(x)$ depending only on x, can be obtained by solution of the 3D Schrödinger equation

$$\left(-\frac{\hbar^2}{2m}\Delta + eV(x)\right)\psi(x,y,z) = (E_C + E)\,\psi(x,y,z)$$

when the extension of the surface element $\mathrm{d}S$ can be considered to be infinite compared to atomic dimensions. In that case the 3D equation is separable with $\psi(x, y, z) = u(x)\, \upsilon(y)\, w(z)$ and for $u(x)$:

$$\left(-\frac{\hbar^2}{2m}\frac{d^2}{dx^2} + eV(x)\right)u(x) = (E_C + E_x)\,u(x) \quad (8)$$

and $(-\hbar^2/2m\;\; d^{\,2}/dy^2\;)\;\upsilon(y) = E_y\;\upsilon(y)$. Similarly $(-\hbar^2/2m\; d^2/dz^2\;)\; w(z) = E_z\; w(z)$. E_x , E_y , E_z denote the components $(\hbar k_x)^2/2m$, … of the total kinetic energy $E(k) = (\hbar k)^2/2m$. E_C defines the zero point for the potential $V(x)$.

For nonplanar surface tip radii approaching atomic dimensions it is more appropriate to consider instead of (8) the full 3D Schrödinger eq. with the radial symmetry of the problem and spherically symmetric $V(r)$. Future work of us will deal with this situation more thoroughly. Tip radii as small as 5nm have already been reported.

3. ENERGY BALANCE IN ELECTRODES

The emitted electrons are replaced by electrons from a reservoir inside the cathode or circuit of temperature T_C . The replacement electrons are scattered into unoccupied levels near the surface. The average electron replacement energy ε_r determines whether heating or cooling of the electrode occurs. If ε_r is lower than the average emitted electron energy, the cathode is cooled during emission, otherwise it is heated by emission. There is an old debate originating from [35] and [36] concerning the average electron replacement energy. In [35] it was argued that ε_r should be slightly below the Fermi-level μ, whereas [36] assumed ε_r to be equal to μ. The theory of [35] was improved in [32] and also results in $\varepsilon_r < \mu$. In [35] and [32] the cathode reservoir temperature is restricted to 0°K.

A further problem with the theory of [35], [32] is the use of the equilibrium distribution $f(E)$ *inside* the emitting cathode for replacement energy current determination. The use of $f(E)$ *inside* the material must strictly lead to zero electron and energy current, since then the integration in (5) (without the factor $D(E_x)$) is not restricted to $k_x > 0$ and all electrons contributing to the current with $k_x > 0$ are exactly cancelled by the same number of electrons with $k_x < 0$. We therefore make use of the non-equilibrium distribution $g(\mathbf{k})$ presented in (2), which leads to nonzero electron and energy current depending on the weak applied electric field and temperature gradient inside the material. The unnatural assumption of zero reservoir temperature then also is not necessary. Similar to (5) the replacement electron current is

$$J_r = e\int_{k_x}\int_{k_y}\int_{k_z}\frac{\hbar k_x}{m}\, g(\mathbf{k})\,\frac{d^3k}{4\pi^3}$$

and now includes full integration over **k**. Inserting (2) with neglected temperature gradient and E-field F_x in x-direction and using the same variable transformation as in (6) leads with the convention $E_C = 0$ to

$$J_r = \frac{8\pi\, e^2\sqrt{2m}}{3\hbar^3}\, F_x\int_0^\infty E^{3/2}\;\tau(E)\left(-\frac{\partial f(E)}{\partial E}\right)dE$$

Again as in (7) the energy replacement current is obtained by weighting the integrand of J_r by E and dividing by e:

$$J_{Er} = \frac{8\pi e\sqrt{2m}}{3\hbar^3} F_x \int_0^\infty E^{5/2}\,\tau(E)\left(-\frac{\partial f(E)}{\partial E}\right) dE \qquad (9)$$

The average electron replacement energy is given by $e\,J_{Er}/J_r$:

$$\varepsilon_r = \int_0^\infty E^{5/2}\,\tau(E)\left(-\frac{\partial f(E)}{\partial E}\right) dE \Big/ \int_0^\infty E^{3/2}\,\tau(E)\left(-\frac{\partial f(E)}{\partial E}\right) dE$$

The expression $(-\partial f(E)/\partial E)$ is a delta-shaped function around μ with a peak of small width also for high temperatures. Thus the integrals for ε_r can be restricted to a small interval around μ where the $\tau(E)$ are essentially constant and therefore cancel. The integrals can then be expanded in a series in T around $T = 0$ by using an expansion of $E^{5/2}$ and $E^{3/2}$ in powers of $(E-\mu)$ of the form $\sum_n H^{(n)}(\mu)\,(E-\mu)^n/n!$. With this $\int H(E)\,(-\partial f(E)/\partial E)\,dE$ can be evaluated to be

$$\int_{-\infty}^{\infty} H(E)\left(-\frac{\partial f(E)}{\partial E}\right) dE = H(\mu) + \sum_{n=1}^{\infty} H^{(2n)}(\mu)\,(k_B T)^{2n}\left(2 - \frac{1}{2^{2(n-1)}}\right)\zeta(2n)$$

where ζ is the Riemann Zeta-function. The lower integration limit has been extended to $-\infty$ with negligible error. With $H(E) = E^{5/2}$ and $E^{3/2}$ a series expansion in $k_B T$ of the nominator and denominator of ε_r is obtained and the rapidly converging series expansion for the fraction ε_r is:

$$\varepsilon_r = \mu + \frac{1}{2}\frac{(\pi k_B T)^2}{\mu} - \frac{11}{120}\frac{(\pi k_B T)^4}{\mu^3} - \frac{19}{1680}\frac{(\pi k_B T)^6}{\mu^5} + \ldots$$

For reasonable temperatures up to 8000 K only the first two terms are significant. This is to be compared with [35]: $\varepsilon_r = \mu - \pi^2 k_B T/(12\ln(2)) - O((k_B T)^2)$. Due to our result $\varepsilon_r(\mu, T)$ is a slowly increasing function of T and for $T > 0$ slightly above the Fermi-level μ, contrary to [35], [32]. μ itself may also depend on temperature. According to our analysis the approximation $\varepsilon_r \approx \mu$, as e.g. used in [16], seems to be correct.

The heat current J_Q due to electrons flowing from the cathode is given by the difference in average energy between emitted and replacement electrons and therefore by the difference of (7) and (9): $J_E - J_{Er}$. Since the electron replacement current J_r must be equal to the emission current (6) by reason of continuity, we have $J_{Er} = \varepsilon_r\,J_e/e$ and:

$$J_Q = \frac{4\pi m}{h^3}\int_0^\infty f(E_C+E)(E_C+E-\varepsilon_r)\left(\int_0^E D(E_x)\,dE_x\right) dE$$

For the complete thermionic converter it is important to take into account also the electron current from the right hand side electrode 2 to electrode 1 in fig.1. This is especially important for low applied voltage V, since for $T_2 > T_1$ a strong backward current can occur. The net electron current J_{en} between the electrodes is obtained by using (6) for the different values μ_1, T_1 and μ_2, T_2 of the electrodes and performing a variable substitution $E+E_{C1,2} \to E$ in the integrals. The difference of both expressions leads to: (10)

$$J_{en} = \frac{4\pi me}{h^3}\int_{E_C}^\infty (f_{\mu 1,T1}(E) - f_{\mu 2,T2}(E))\left(\int_{E_C}^E D(E_a)dE_a\right) dE$$

The transmission $D(E_a)$ is here expressed as function of the absolute electron energy $E_a = E_C + E_x$ in x-direction. E_C denotes the maximum of both electrodes conduction band edges: $E_C = \mathrm{Max}(E_{C1}, E_{C2})$. Also use has been made of the independence of $D(E_a)$ on the electron's direction, which is true for any shape of the potential barrier provided E_a is the same for both directions [37]. $D(E_a)$ is zero for $E_a < E_C$, since no transmission is possible in this case. When considering only J_e without backward current, strictly speaking an additional factor $(1 - f_{\mu 2,\,T2})$ should be included in (6) to take into account the occupied electron levels in the collector electrode. However, for the net current (10) this factor cancels, since $f_1(1-f_2) - f_2(1-f_1) = f_1 - f_2$. J_{en} depends on V through the the Fermi-level $\mu_2 = \mu_1 - e$ V (see fig.1, V in Volt) and the function $D(E_a)$, since V influences the barrier $V(x)$ and the barrier in turn D.

Now it is easy to gain the net heat flow from electrode 1 to 2 by weighting the net current (10) with $(E-\varepsilon_r)$ and dividing by e :

$$J_{Qn} = \frac{4\pi m}{h^3}\int_{E_C}^\infty \frac{(f_{\mu 1,T1}(E) - f_{\mu 2,T2}(E))\,(E-\varepsilon_r(\mu_1,T_1))}{\left(\int_{E_C}^E D(E_a)dE_a\right)} dE \qquad (11)$$

This is the cooling power (in [W/m^2]) for electrode 1 or the heat current density leaving electrode 1. The heat current which arrives at electrode 2 is obtained by replacing in (11) $\varepsilon_r(\mu_1, T_1)$ by $\varepsilon_r(\mu_2, T_2)$. The difference of both currents is $P = V\,|J_{en}|$, the electrical power (in [W/m^2]) needed for the operation of the thermionic converter as refrigerator. In section 5 Joule heating in the electrodes and contact resistances will also be included.

4. PURE THERMIONIC EMISSION

For thermionic emission it is assumed that no tunnelling of particles occurs. All emitted electrons have to have a energy higher than the maximum $V_{\max}$ (in eV) of the potential surface barrier. In this classical approximation the transmission coefficient $D(E)$ is always zero for $E < V_{\max}$ and $D(E) = 1$ for $E \geq V_{\max}$. Inserting these values for $D(E)$ into (10), (11) the integration can be performed exactly analytically. The result is expressed by polylogarithm functions $\mathrm{Li}_n[z] = \sum_{i=1} z^i/i^n$ with $z = -\exp(-(V_{\max}-\mu_{1,2})/k_B T_{1,2})$. We derived the following formulas, which are probably known and valid for all real x, to obtain that result:

$$\mathrm{Li}_2[-\exp(-x)] = -(\pi^2 + 3x^2 + 6\,\mathrm{Li}_2[-\exp(+x)])/6$$
$$\mathrm{Li}_3[-\exp(-x)] = +(\pi^2 x + x^3 + 6\,\mathrm{Li}_3[-\exp(+x)])/6$$

For $(V_{\max}-\mu_{1,2})$ on the order of material workfunctions and T below several 1000 K the magnitude of z is so small that the Li(z) functions can be very accurately approximated by z. Then the result for the net electron and heat current is:

$$J_{en} = \frac{4\pi me k_B^2}{h^3} \times \left(T_1^2 \exp(-(V_{\max}-\mu_1)/k_B T_1) - T_2^2 \exp(-(V_{\max}-\mu_2)/k_B T_2\right)$$

$$J_{Qn} = 4\pi\, m k_B^2 / h^3 \qquad (12)$$
$$\times \begin{pmatrix} T_1^2 (2k_B T_1 + V_{\max} - \varepsilon_r(\mu_1, T_1)) \exp(-(V_{\max} - \mu_1)/k_B T_1) \\ -T_2^2 (2k_B T_2 + V_{\max} - \varepsilon_r(\mu_1, T_1)) \exp(-(V_{\max} - \mu_2)/k_B T_2) \end{pmatrix}$$

The first term of J_{en} (current from electrode 1 to 2) is for $V_{\max} = W + \mu_{1,2}$ the traditional thermionic Richardson current, which is usually inferred in another way. The expression for J_{Qn} corresponds, likewise for $V_{\max} = W + \mu_{1,2}$, to the result in [10], however, (12) is more general. Very low $V_{\max}$ can be obtained for increased voltages in nano-gap devices. Our analysis suggests that in this case our original analytical formulas with polylogarithms should be used. On the other hand, the tunnelling contribution in nano-gap devices is not negligible, so that the premises $D(E) = \Theta(E - V_{\max})$ is not fulfilled.

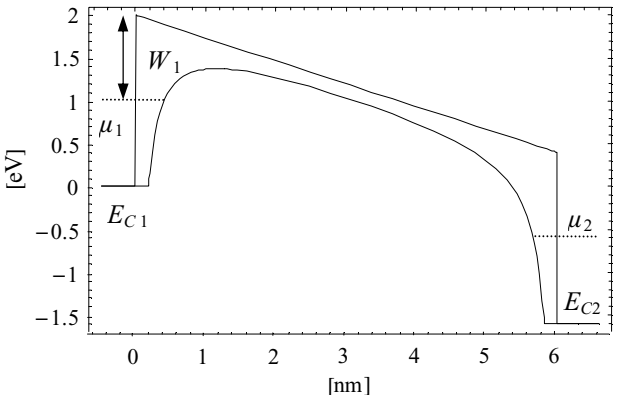

Figure 2: Potential profile (13) in d = 6nm vacuum gap with voltage V_{bias}=1.6V, W_1, W_2 = 1eV, E_{C1}=0, E_{C2}=E_{C1}−$e\,V_{bias}$, μ_1=1eV. Top curve represents the first two terms of (13).

5. COMBINED FIELD AND THERMIONIC EMISSION - NANOMETER GAP DESIGN -

In ref. [16] a theoretical investigation of nano-gap thermionic devices was performed. For nanometer distances d of the plane electrodes multiple image forces become important. One free electron in the vacuum gap causes an image of opposite charge in electrode 1 and 2. The images themselves cause other image charges in the electrodes which then cause new image forces. Thus an infinite series is obtained for the gap potential with applied voltage V_{bias}:

$$V_d(x) = \frac{W+\mu}{e} - V_{bias}\frac{x}{d} - \frac{e}{4\pi\varepsilon_0}\left(\frac{1}{4x} + \frac{1}{2}\sum_{n=1}^{\infty}\left(\frac{nd}{n^2d^2 - x^2} - \frac{1}{nd}\right)\right)$$

A factor ½ has to be incorporated, because the mirror charge position is not constant, when the electron's position x varies. We included the workfunction of the second electrode W_2 and succeeded to sum the infinite series exactly analytical. V_d then reads:

$$V_d(x) = \frac{W_1+\mu_1}{e} - \frac{x}{d}(V_{bias} + (W_1 - W_2)/e) \qquad (13)$$
$$-\frac{e}{4\pi\varepsilon_0}\left(\frac{1}{4x} - \frac{C}{2d} - \frac{1}{4d}(\psi(1-\frac{x}{d}) + \psi(1+\frac{x}{d}))\right)$$

Here C = 0.5772… denotes Euler's constant, ψ is the digamma function (logarithmic derivative of the gamma-function). The potential exhibits singularities at both electrodes at x =0 and x =d, which are not real. We therefore limit the potential to E_{C1} near x =0 for $V_d(x) < E_{C1}$, and to E_{C2} near x =d for $V_d(x) < E_{C2}$. Figure 2 shows as an example the potential shape for d = 6 nm. As can be seen from fig. 2 a considerable reduction of the potential maximum from originally 2 V to $V_{\max}$ = 1.375 V occurs, which is due to the image forces (the 2nd line in (13)). This effect is for similar V_{bias} nearly negligible in case of large gaps with d in the region of µm or mm.

The electron transmission probabilities $D(E)$ are needed in the expressions (10), (11) for the currents, in order to calculate the device performance. The theory of field and thermionic emission are combined by calculating $D(E)$ precisely numerically from (8) as interpolated function. Using (13) for the Schrödinger-equation (8), the wave function $u(x)$ can be obtained for any given electron energy $E = E_C + E_x$ in the x-interval (0, d). In the electrodes region $x < 0$ and $x > d$, $V(x)$ is constant (= E_{C1} , E_{C2}) with plane wave functions $u(x)$, due to the free electron model. A transmitted wave for an incident electron from right to left is of the form in $x < 0$: $S\exp(-i\,x\sqrt{2m(E-E_{C1})}/\hbar)$. This gives with S = 1 at x = 0 the start condition for $u(x)$ in (8). For $x > d$ a superposition of incident and reflected wave is used: $Y\exp(-i\,x\sqrt{2m(E-E_{C2})}/\hbar) + R\exp(i\,x\sqrt{2m(E-E_{C2})}/\hbar)$. Y and R are determined by the continuity condition for $u(x)$ and $u'(x)$ at $x = d$. The transmission coefficient then is given by $D(E) = 1 - |R/Y|^2$.

In fig.3 a result of this calculation is displayed. For every value E the differential equation (8) was solved numerically with a standard package and $D(E)$ calculated subsequently. The complete function $D(E)$ in fig.3 is created as interpolated function within 16 sec on a 3 GHz PC.

The Wentzel-Kramers-Brillouin method (WKB, [34]) is often used for an approximate solution of the 1D eq. (8). Within this approximation $D(E)$ can be represented as:

$$D(E) = \exp\left(-\frac{2}{\hbar}\int_{x1}^{x2}\sqrt{2m(eV(x)-E)}\,dx\right).$$

$x1$ and $x2$ are the turning points of the problem, i.e. $V(x1,\ x2) = E$. For E exceeding the potential maximum $V_{\max}$, $x1$ equals $x2$ and $D(E)$ is set to the classical value 1. In that region the WKB approximation is no longer valid. Contrary to classical mechanics there is a non vanishing probability for the electron to be reflected, also when $E > V_{\max}$, in the same way as there is a non vanishing probability for transmission, when $E < V_{\max}$. Therefore $D(E) < 1$ also for $E > V_{\max}$. The WKB-approximation in fig.3 is not bad. Its threshold voltage is near to $V_{\max}$ = 1.375 V. Surprisingly the threshold of the exact curve is higher, above

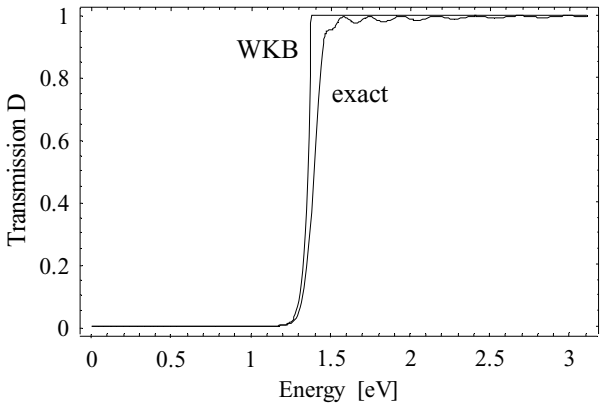

Figure 3: Transmission probability $D(E)$ for potential profile (13) with V_{bias}=1.6V (fig.2). Exact curve by numerical solution of Schrödinger eq. (8), WKB-curve by WKB-method.

1.4V. For other barrier shapes the WKB approximation can fail severely, as can easily be shown by comparison with analytical solvable cases.

The standard numerical algorithm for solving the Schrödinger eq. (8) fails, if the gap width d increases. In the regions with $E > e\,V(x)$ the wave function $u(x)$ is highly oscillatory, which necessitates an extraordinarily large number of x-steps. Therefore $V(x)$ is approximated by a piecewise constant function and (8) is solved analytically in each constant interval with continuity conditions for $u(x)$, $u'(x)$ at the borders of the intervals. The solution is obtained recursively very rapidly, so that the $D(E)$ function in fig.3 can be calculated within 1 sec with nearly equal accuracy. However, this method fails again for other barrier shapes to be considered later. So a similar method was developed with piecewise linear approximation to $V(x)$. The solution in each linear interval of $V(x)$ is given by Airy-functions which bears some numerical subtleties. Nevertheless, with this the most reliable method was obtained for solving (8) for all geometry and bias conditions. The $D(E)$ function can be calculated in typically less than 3 sec with this method.

In fig.4 the net heat current from electrode 1 (cooling power) according to (11) is shown for different separations of the electrodes and different bias voltages. The result looks promising and is qualitatively similar to [16]. Our result includes exact $D(E)$ functions instead of WKB approximations, the presence of the backward current from the 2nd electrode and a precise consideration of all emission directions because of (6), instead of effectively considering lateral currents by a term $k_B\,T$. The temperature of elecrode 1 to be cooled is 405°K, and of the collector electrode 2: T_2 = 450 °K.

Essential for the assessment of the thermionic refrigerator performance, however, is the relation of the cooling power to the electrical power $P = V_{bias}\,|J_{en}|$ needed for device operation, which is expressed by the "coefficient of performance" $\phi = J_Q / P$. ϕ is limited by the Carnot-efficiency $\phi_C = T_2/(T_2 - T_1)$ (= 9 for fig.5). Figure 5 shows

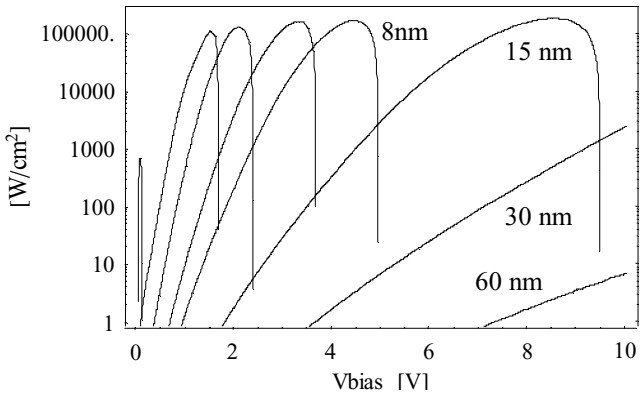

Figure 4: Cooling power of thermionic refrigerator for plane elect. distance: 2, 3, 4, 6, 8, 15, 30, 60 nm. T_1=405, T_2=450K

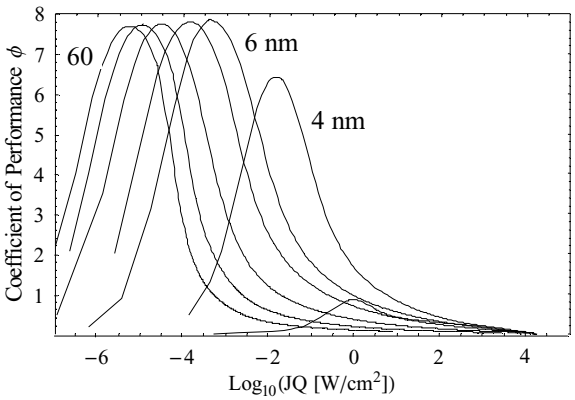

Figure 5: CoP of thermionic refrigerator for plane elect. distance: 3, 4, 6, 8, 15, 30, 60 nm. T_1=405 K, T_2=450 K.

the CoP plotted against the cooling power for the different electrode separations. Very high CoP near Carnot efficiency, much higher than for thermoelectric devices, can be obtained for extremely low cooling powers < 10^{-1} W/cm^2 . However, for cooling powers of technical interest > 1 W/cm^2 the CoP is below or at best similar to what can be achieved by conventional bulk-material thermoelectric devices.

Additional Joule heating J_J in the cathode and its contact resistance has also been taken into account in the CoP in fig.5. For a contact resistance and internal electrode resistance R the cooling power is reduced to $J_Q - J_J = J_Q - R\,J_{en}^2$ and the operation power is increased by $R\,J_{en}^2$. Thus: $\phi = (J_Q - R\,J_{en}^2) / (V_{bias}\,|J_{en}| + R\,J_{en}^2)$. We assumed an effective R of 10^{-6} Ω for 1 cm^2 device area. The Joule losses have little or negligible influence except for extremely small spacing of d = 2 nm, when very high electrical current densities occur. The CoP is of negative sign in this case (Joule heating larger than cooling) and therefore not represented in fig.5.

Figure 6 shows the same as in fig.5 for largely increased temperatures of T_1 = 900 °K and T_2 = 1000 °K. The Carnot-efficiency is again 9. Now very large CoP at much higher cooling powers result. The CoP are even better than for advanced nanostructured thermoelectric devices. (Again the performance for$d$ = 2 nm is destroyed by Joule heating.)

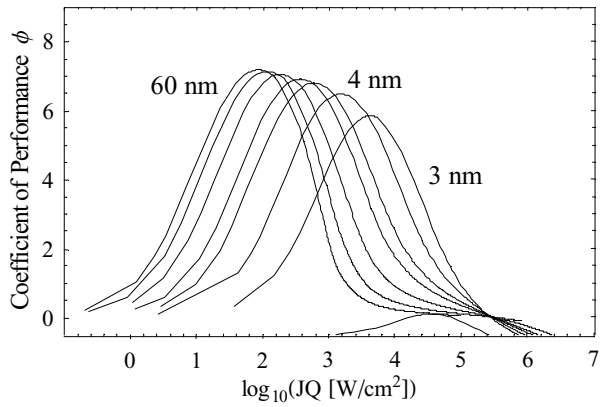

Figure 6: CoP of thermionic refrigerator for plane elect. distance: 2, 3, 4, 6, 8, 15, 30, 60 nm. T_1=900 K, T_2=1000 K.

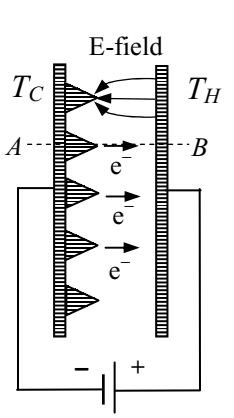

Figure 7: Thermionic cooler with electron field emission by enhanced electric field at tips.

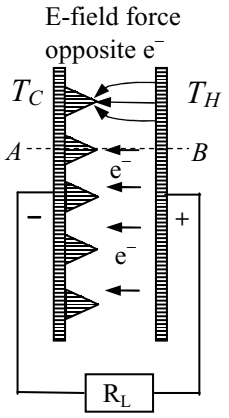

Figure 8: Device in generator mode. E-field opposes e$^-$ which is driven by $T_H > T_C$.

However, this temperature region is not suited for electronic cooling applications. Our theory allows for a calculation of the generator efficiency by the same set of data as obtained for cooling. For the same electrode temperatures the current reverses in the generator mode for very low positive bias voltage, because of $T_2 > T_1$. The device then delivers power to the external circuit. The generator efficiency η is defined as delivered power $P = V_{bias} |J_{en}|$ divided by the heat current from the 2nd (hot) electrode. The Carnot efficiency is $\eta_C = (T_2 - T_1) / T_2$. As in the cooling case η is near η_C with generated powers up to 500 W/cm^2. However, for the more interesting low temperature case (T_1 = 405 K, T_2 = 450 K) the generated power-densities are very small (< 10^{-2} W/cm^2), when good efficiencies are to be obtained.

6. EMISSION FROM NANOTIP ELECTRODES

Figure 7 shows a thermionic cooler with numerous metal tips on the cathode electrode. Due to the small tip radii the electric field is enhanced strongly at the tips. This leads to a deformed electrostatic potential shape with very small barrier width, as shown in fig. 9 along the line A-B, so that electrons of lower energy can tunnel by field emission instead of thermionic emission. Devices similar to fig.7 have been devised in vacuum microelectronics usually with inclusion of a gate electrode to control the current flow [19, 20, 21]. The advantages of vacuum microelectronics include high operation temperatures, radiation hardness, and use for very high frequencies. Also flat panel displays are considered for this technique. Improved properties and long term reliability are expected with carbon-nano-tubes [22] or diamond coated tips [23, 24], however, our work is restricted to metal and semiconductor field emission surfaces. Structures like that in fig.7 have been proposed in [25], [26] for cooling applications. In the inverse operation mode as generator shown in fig. 8, the electric field exerts a force in opposite direction to the electron movement.

In case of a cone with tip radius r_0 which emits electrons, we assume a 3D radial symmetric potential near the

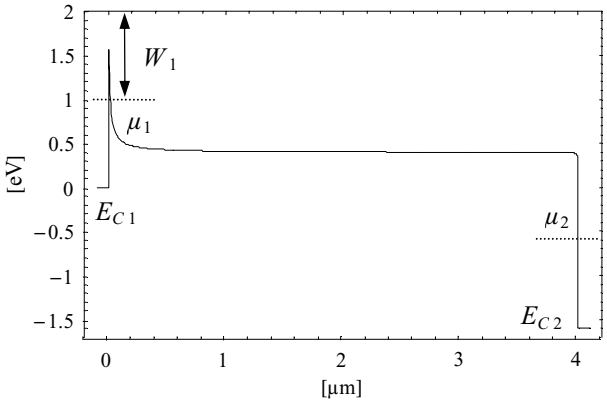

Figure 9: Potential profile (14) for d =4μm and nanotip r_0 = 10nm, bias V_{bias}=1.6V, W_1, W_2 =1eV, μ_1=1eV, μ_2= $\mu_1 - e\,V_{bias}$

surface of the spherical tip, which leads to [28, 25]:

$$V_r(x) = \frac{W_1 + \mu_1}{e} - \frac{(V_{bias} + (W_1 - W_2)/e)}{d}\left(1 - \frac{r_0}{x + r_0}\right) - \frac{e}{4\pi\varepsilon_0}\frac{\varepsilon - 1}{\varepsilon + 1}\left(\frac{r_0}{2x(2r_0 + x)} + \frac{1}{4(d - x)}\right) \qquad (14)$$

$V_r(x) = E_{C1}$ for $x < 0$, $V_r(x) = E_{C2}$ for $x > d$.

x denotes the normal distance from the spherical tip. The image potential for the sphere as given by [25, 33] has been added and also the image potential for the plane electrode in the 2nd line. ε is the dielectric constant of the emitter. In case of metals the factor $(\varepsilon - 1)/(\varepsilon + 1)$ has to be omitted. d denotes the distance from the tip to the (nearly) plane collector electrode. Contrary to the last section, d now assumes values in the μm or mm range, to make possible a technological realisation. The calculation of the potential for the tip array of fig.7 is obviously a 3D problem but at least in a neighbourhood along the lines AB $V_r(x)$ gives a useful 1D approximation. Figure 9 shows $V_r(x)$ for a tip radius of 10 nm. The width of the peak at μ_1 = 1eV is 20nm, so the reduction of the peak height from 2eV to V_{max} = 1.572 eV may be more important for improved emission.

We can now apply the same formalism as in section 5 to calculate electron and heat currents at the field emitting tips. The fraction of the tip area of the array compared to the device area is taken into account by a reduction of J_Q to 6% in fig.10. Figure 10 shows the result for high temperatures (T_1 = 900K, T_2 = 1000K). The CoP exceeds that of thermoelectric devices by far with good power densities. For the low temperature case (405K, 450K), similar to fig. 5, much too small power densities below 10^{-3} W/cm^2 arise.

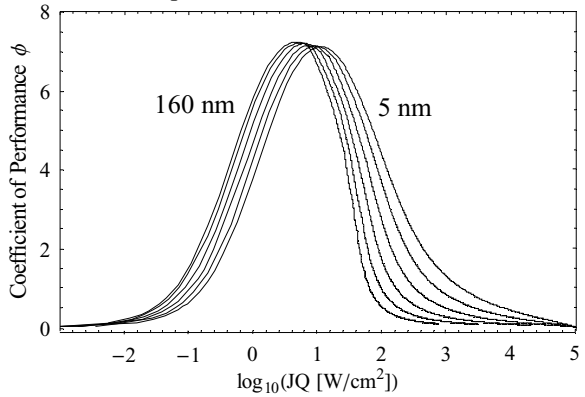

Figure 10: CoP of nanotip thermionic refrigerator for tip radii: 5, 10, 20, 40, 80, 160 nm. T_1=900 K, T_2=1000 K.

7. REFERENCES

[1] A. Shakouri, Y. Zhang, "On-Chip Solid-State Cooling for Integrated Circuits Using Thin-Film Microrefrigerators," IEEE Trans. on Comp. and Pack. Technol., vol.28, 2005, pp.65-69.

[2] J.W. Vandersande, J.-P. Fleurial, "Thermal management of power electronics using thermoelectric coolers," Proc. of Intern. Conf. on Thermoelectrics 1996 (ICT1996), pp. 252-255.

[3] G.S. Nolas, J. Sharp, H.J. Goldsmid, *Thermoelectrics, Basic Principles and New Materials Developments*, Berlin 2001.

[4] M.S. El-Genk et al., Proc of Intern. Conf. on Thermoelectrics 2003 (ICT2003), pp.417-420.

[5] M. Strasser, R. Aigner, M. Franosch, G. Wachutka, Sensors and Actuators A, A97-98, 2002, pp. 535-542.

[6] X. Fan et al., "SiGeC/Si superlattice microcoolers," Applied Physics Letters, vol.78(11), 2001, pp.1580-1582.

[7] R. Venkatasubramanian et al., "Thin-film thermoelectric devices with high room-temperature figures of merit," Nature, vol. 413, Oct. 2001, pp. 597-602.

[8] S. Ghamaty, J.C. Bass et al., "Quantum well thermoelectric devices and applications," Proc of Intern. Conf. on Thermoelectrics 2003 (ICT2003), pp. 563-566.

[9] S.W. Angrist, "Direct Energy Conversion," 3rd edition, Allyn and Bacon, Boston, 1977.

[10] G.D. Mahan, "Thermionic refrigeration," J. Appl. Phys. 76, 1994, pp. 4362-4366.

[11] G.D. Mahan et al., "Multilayer thermionic refrigerator and generator," J. Appl. Phys. 83, 1998, pp.4683-4689.

[12] A. Shakouri, J.E. Bowers, "Heterostructure integrated thermionic coolers," Applied Physics Letters, vol.71(9), 1997, pp.1234-1236.

[13] A. Shakouri et al., "Thermionic emission cooling in single barrier heterostructures," Applied Physics Letters, vol.74(1), 1999, pp.88-89.

[14] A. Shakouri et al., "Thermoelectric Effects in Submicron Heterostructure Barriers," Microscale Thermophysical Engineering, vol.2, 1998, pp.37-47.

[15] M.D. Ulrich, P.A. Barnes, C.B. Vining, "Effect of contact resistance in solid state thermionic refrigeration," J. Appl. Phys. 92, 2002, pp. 245-247.

[16] Y. Hishinuma et al., "Refrigeration by combined tunneling and thermionic emission in vacuum: Use of nanometer scale design," Applied Physics Letters, vol.78(17), 2001, pp.2572-2574.

[17] A. Tavkhelidze et al., "Electron tunneling through large area vacuum gap – preliminary results, Proc. of Intern. Conf. on Thermoelectrics 2002 (ICT2002), pp. 435-439.

[18] http://www.borealis.gi

[19] I. Brodie, P.S. Schwoebel, "Vacuum Microelectronic Devices," Proc. of The IEEE, vol.82, no.7, 1984, pp. 1006-1034.

[20] C.A. Spindt, I. Brodie, et al., "Physical properties of thin-film emission cathodes with molybdenum cones," J. Appl. Phys. 47, no.12, 1976, pp. 5248-5263.

[21] J.A. Nation et al., "Advances in Cold Cathode Physics and Technology," Proc. of The IEEE, vol.87, (5), 1999, pp. 865-889.

[22] O. Gröning et al., "Prospects and Limitations of Carbon Nanotube Field Emission Electron Sources, "Chimia 56, 2002, pp. 553-561.

[23] M.W. Geis et al., "A new surface electron-emission mechanism in diamond cathodes," Nature, vol. 393, 1998, pp. 431-435.

[24] P. Lerner, P.H. Cutler, N.M. Miskovsky, "Cold-cathode Emitter Based on a Metal-diamond Tunneling Junction," IEEE Trans. On Dielectrics and Electrical Insulation, vol. 4, no.6, 1997, pp. 827-829.

[25] T.S. Fisher, D.G. Walker, "Thermal and Electrical Energy Transport and Conversion in Nanoscale Electron Field Emission Process," Journal of Heat Transfer, vol.124, 2002, pp. 954-962.

[26] Y.C. Gerstenmaier, "Report on thermoelectric and thermionic generators and coolers," Siemens AG, July 2004.

[27] R.H. Good, E.W. Mueller, "Field Emission" in Handbuch der Physik, vol. 21, Berlin 1956, pp. 176-231.

[28] R. Gomer, "Field Emission and Field Ionization," Harvard Univ. Press, Cambridge, Mass., 1961.

[29] R.H. Fowler, L.W. Nordheim, "Field Emission from Metallic Surfaces," Proc. R. Soc. London, A119, 1928, pp.173-181.

[30] N.W. Ashcroft, N.D. Mermin, *Solid State Physics*, Holt, Rinehart, Winston, Philadelphia, PA 1976.

[31] A.A. Grinberg, "Thermionic emission in heterosystems with different effective electronic masses," Phys. Rev. B, vol.33, no. 10, 1986, pp. 7256-7258.

[32] M.S. Chung, P.H. Cutler, N.M. Miskovsky, T.E. Sullivan, "Energy exchange processes in electron emission at high fields and temperatures," J. Vac. Sci. Technol. B12, 1994, pp. 727-736.

[33] K.L. Jensen, E.G. Zaidman, Appl. Phys. Lett. 63 (5), August 1993, 702-704.

[34] S.C. Miller, R.H. Good, "A WKB-Type Approx. to the Schrödinger Eq.," Phys. Rev. vol. 91, no.1, 1953, pp. 174-179.

[35] G.M. Fleming, J.E. Henderson, "The Energy Loss Attending Field Current and Thermionic Emission of Electrons from Metals," Phys. Rev. vol. 58, 1940, pp. 887-894.

[36] W.B. Nottingham, "Remarks on Energy Losses Attending Thermionic Emission of Electrons from Metals ," Phys. Rev. vol. 59, 1941, pp. 906-907.

[37] A. Messiah, *Quantum Mechanics*, Vol. I, North-Holland, Amsterdam, 1972.